Crystal Structure and Site-Specific Mutagenesis of Pterin-Bound Human Phenylalanine Hydroxylase[†,‡]

Heidi Erlandsen,[§] Elisa Bjørgo,[||,⊥] Torgeir Flatmark,[||] and Raymond C. Stevens*[,§]

Departments of Molecular Biology and Chemistry, The Scripps Research Institute, 10550 North Torrey Pines Road, La Jolla, California 92037, Department of Biochemistry and Molecular Biology, University of Bergen, Årstadveien 19, N-5009 Bergen, Norway, and Biotechnology Centre of Oslo, P.O. Box 1125, Blindern, N-0316 Oslo, Norway

Received November 2, 1999; Revised Manuscript Received December 16, 1999

ABSTRACT: The crystal structure of the dimeric catalytic domain (residues 118−424) of human PheOH (hPheOH), cocrystallized with the oxidized form of the cofactor (7,8-dihydro-L-biopterin, BH_2), has been determined at 2.0 Å resolution. The pterin binds in the second coordination sphere of the catalytic iron (the C4a atom is 6.1 Å away), and interacts through several hydrogen bonds to two water molecules coordinated to the iron, as well as to the main chain carbonyl oxygens of Ala322, Gly247, and Leu249 and the main chain amide of Leu249. Some important conformational changes are seen in the active site upon pterin binding. The loop between residues 245 and 250 moves in the direction of the iron, and thus allows for several important hydrogen bonds to the pterin ring to be formed. The pterin cofactor is in an ideal orientation for dioxygen to bind in a bridging position between the iron and the pterin. The pterin ring forms an aromatic π-stacking interaction with Phe254, and Tyr325 contributes to the positioning of the pterin ring and its dihydroxypropyl side chain by hydrophobic interactions. Of particular interest in the hPheOH·BH_2 binary complex structure is the finding that Glu286 hydrogen bonds to one of the water molecules coordinated to the iron as well as to a water molecule which hydrogen bonds to N3 of the pterin ring. Site-specific mutations of Glu286 (E286A and E286Q), Phe254 (F254A and F254L), and Tyr325 (Y325F) have confirmed the important contribution of Glu286 and Phe254 to the normal positioning of the pterin cofactor and catalytic activity of hPheOH. Tyr325 also contributes to the correct positioning of the pterin, but has no direct function in the catalytic reaction, in agreement with the results obtained with rat TyrOH [Daubner, S. C., and Fitzpatrick, P. F. (1998) *Biochemistry 37*, 16440−16444]. Superposition of the binary hPheOH·BH_2 complex onto the crystal structure of the ligand-free rat PheOH (which contains the regulatory and catalytic domains) [Kobe, B., Jennings, I. G., House, C. M., Michell, B. J., Goodwill, K. E., Santarsiero, B. D., Stevens, R. C., Cotton, R. G. H., and Kemp, B. E. (1999) *Nat. Struct. Biol. 6*, 442−448] reveals that the C2′-hydroxyl group of BH_2 is sufficiently close to form hydrogen bonds to Ser23 in the regulatory domain. Similar interactions are seen with the hPheOH·adrenaline complex and Ser23. These interactions suggest a structural explanation for the specific regulatory properties of the dihydroxypropyl side chain of BH_4 (negative effector) in the full-length enzyme in terms of phosphorylation of Ser16 and activation by L-Phe.

The mononuclear non-heme iron(II)-containing enzyme phenylalanine hydroxylase (PheOH,[1] phenylalanine 4-monooxygenase, EC 1.14.16.1) hydroxylates L-phenylalanine (L-Phe) into L-tyrosine (L-Tyr) in the presence of the cofactors (6*R*)-L-*erythro*-5,6,7,8-tetrahydrobiopterin (BH_4) and dioxygen (for reviews, see refs *1*−*4*). During the hydroxylation reaction, the BH_4 cofactor undergoes a two-electron oxidation to 4a-hydroxydihydrobiopterin (pterin 4a-carbinolamine) which is subsequently dehydrated to quinonoid dihydropterin (q-BH_2) by 4a-carbinolamine dehydratase (EC 4.2.1.96), before it is reduced by dihydropteridine reductase (EC 1.6.99.7) (Scheme 1). The quinonoid dihydropterin can alternatively isomerize to 7,8-dihydro-L-biopterin (BH_2).

PheOH is structurally and functionally homologous to tyrosine hydroxylase (TyrOH, tyrosine 3-monooxygenase, EC 1.14.16.2) and tryptophan hydroxylase (TrpOH, tryptophan 5-monooxygenase, EC. 1.14.16.4), comprising the family of the tetrahydrobiopterin-dependent aromatic amino acid hydroxylases. While PheOH is critical for catabolizing phenylalanine, TyrOH and TrpOH catalyze important rate-limiting steps in the biosynthesis of neurotransmitters and hormones. The three enzymes have a three-domain structure,

[†] The studies were supported by The Scripps Research Institute (H.E. and R.C.S.), the Research Council of Norway (E.B. and T.F.), Rebergs legat (T.F.), the Novo Nordisk Foundation (T.F.), and the European Commision (T.F.).

[‡] The coordinates have been deposited with the Protein Data Bank with ID code 1DMW.

* To whom correspondence should be addressed. E-mail: stevens@scripps.edu. Telephone: (858) 784-9416. Fax: (858) 784-9483.

[§] The Scripps Research Institute.

[||] University of Bergen.

[⊥] Biotechnology Centre of Oslo.

[1] Abbreviations: PheOH, phenylalanine hydroxylase; hPheOH, human phenylalanine hydroxylase; rPheOH, rat phenylalanine hydroxylase; TyrOH, tyrosine hydroxylase; rTyrOH, rat tyrosine hydroxylase; TrpOH, tryptophan hydroxylase; BH_2, 7,8-dihydro-L-biopterin; BH_4, (6*R*)-L-*erythro*-5,6,7,8-tetrahydrobiopterin; L-Phe, L-phenylalanine; L-Tyr, L-tyrosine; K'_m, apparent K_m; V'_{max}, apparent V_{max}.

10.1021/bi992531+ CCC: $19.00
Published on Web 02/09/2000

Scheme 1: Reaction of Phenylalanine Hydroxylase and Regeneration of Cofactor[a]

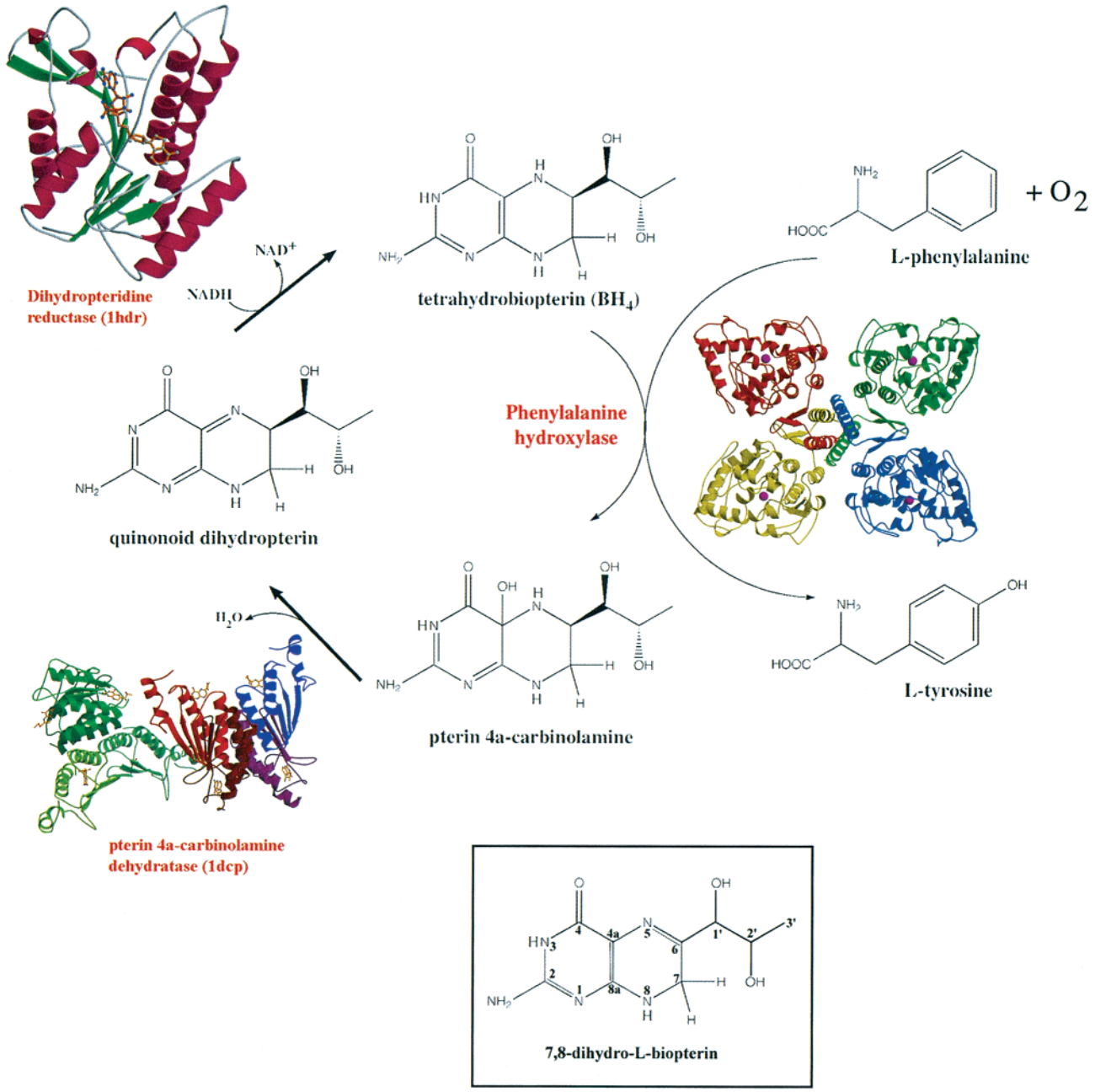

[a] The structure of 7,8-dihydro-L-biopterin is shown.

with an N-terminal regulatory domain (hPheOH residues 1−142), a central catalytic domain (hPheOH residues 143−410) which includes the active site iron with a 2-His-1-Glu facial triad (*5*, *6*) of ligated residues, and a C-terminal tetramerization domain (hPheOH residues 411−452) (*7*−*10*). The crystal structure of rTyrOH with 7,8-dihydro-L-biopterin (BH_2), an analogue of the natural cofactor BH_4, has recently been reported (*11*), and the pterin was found to be positioned in the second coordination sphere of the iron. The pterin binding site has been proposed to be in a highly conserved region in all the aromatic amino acid hydroxylases (*3*, *12*).

Here we present the crystal structure of the corresponding binary complex between hPheOH and BH_2. Site-specific mutagenesis of the doubly truncated form of hPheOH used in the crystallographic study was performed to confirm or exclude the involvement of some of the active site residues in pterin binding and catalysis.

EXPERIMENTAL PROCEDURES

Crystallization and Data Collection. The doubly truncated form of human PheOH was expressed and purified as previously described (*13*, *14*). The crystals were grown as previously described (*15*), but with some modifications of the crystallization protocol. Crystallization conditions included the addition of 10% (v/v) of the cryoprotectant ethylene glycol. A saturated solution of 7,8-dihydro-L-biopterin (BH_2) (Dr. B. Schircks Laboratories, Jona, Switzerland) was made by dissolving the solid BH_2 in 5 mM HCl and then sonicating the solution for approximately 10 min. The resultant solution with a BH_2 concentration of approximately 10−12 mM [as measured at a wavelength of

Table 1: Data Collection, Processing, and Final Model Statistics[a]

space group	$C222_1$
unit cell parameters (Å)	$a = 66.4$, $b = 108.0$, $c = 124.6$
resolution range (Å)	20.0−2.0 (2.07−2.00)
no. of reflections	29570 (2093)
redundancy	4 (2)
completeness (%)	96.5 (69.2)
R_{sym} (I) (%)	7.2 (31.1)
R_{cryst} (%)	20.0
R_{free} (%)	24.5
no. of structural waters in the model	152
overall B-factor (Å^2)	31.9
B-factor for 7,8-dihydro-L-biopterin (Å^2)	33.4
occupancy for 7,8-dihydro-L-biopterin	0.5
estimated coordinate error (Luzatti plot) (Å)	0.23
rms deviation for bond lengths (Å)	0.015
rms deviation for bond angles (deg)	1.7
rms deviation for dihedral angles (deg)	22.1
rms deviation for improper angles (deg)	1.13

[a] The values in parentheses are for the last resolution bin.

330 nm using an extinction coefficient of 6.2 (*16*)] was then neutralized and added to the crystallization reservoir at twice the concentration of that in the drop. On the basis of UV spectroscopy and mass spectrometry, the pterin solution was found to be quite stable, although minor species possibly corresponding to some oxidation products were seen. Experiments where 7,8-BH_2 was added to the protein solution only prior to setting up the hanging drop failed to produce suitable crystals. The final concentration of BH_2 that was used was ~1 mM (in the drop). The reservoir solutions also contained 20−30% (w/v) polyethylene glycol 2000 and 40−80 mM PIPES buffer (pH 6.8). The protein concentration was 4.5 mg/mL (in the drop). The hanging drop contained 5 μL from the reservoir solution mixed with 5 μL of the protein solution. The crystals grew within 1−2 days and with a size (1.0 mm × 0.5 mm × 0.1 mm) and morphology similar to those of the original native crystals (*15*). Attempts at creating a higher concentration of BH_2 for crystallization experiments were unsuccessful.

The hPheOH·BH_2 crystals were frozen in liquid nitrogen directly from mother liquid prior to data collection. Ninety frames with a rotation angle of 1° and a crystal-to-detector distance of 200 mm were collected at the Stanford Synchrotron Radiation Laboratory (SSRL) beamline 7-1 with a MAR detector (MAR Research) and a wavelength of 1.08 Å. A cold stream of nitrogen was used to cool the crystal to 100 K. The images were processed with DENZO and SCALEPACK (*17*). The binary complex crystallized in the same space group as the native crystals ($C222_1$), but with cell dimensions ($a = 66.4$ Å, $b = 108.0$ Å, and $c = 124.6$ Å) slightly shorter than the native room-temperature data. The completeness of the data between 20 and 2.0 Å is 96.5% with an R_{merge} of 7.2%. The completeness and quality of the data are presented in more detail in Table 1.

Model Building and Refinement. The structure of the native doubly truncated form of hPheOH (*7*) was used as a model to calculate a difference electron density map ($F_{obs} - F_{calc}$). The position of BH_2 was relatively clear in the initial difference map (with no refinement performed), and became even better after initial rigid body refinement and energy minimization of the native model against the measured data. Energy minimization and refinement were carried out with the program CNS (version 0.4) (*18*). Ten percent of the data were set off for cross-validation of refinement [the R_{free} value (*19*)]. A maximum likelihood target was used for refinement, and a bulk solvent correction with anisotropic B-factor correction was employed.

The program O (*20*) was used to manually fit the differences from the native structure into the experimental electron density, using CCP4 (*21*) omit maps with 15-residue stretches omitted. Composite CNS (*22*) σ-weighted $2F_{obs} - F_{calc}$ and $F_{obs} - F_{calc}$ omit maps were also used, with spheres of 8−10% of the atoms omitted from the model. The final model includes residues 118−424, the active site iron, the BH_2 cofactor analogue, and 152 structural water molecules. The structure has been refined to a crystallographic R-factor of 20.0% and an R_{free} of 24.6%. The details of the final model statistics are presented in Table 1.

Site-Specific Mutagenesis. The mutations were introduced into the doubly truncated form of the wt-hPheOH cDNA (ΔN102/ΔC24-hPheOH) by PCR-based site-specific mutagenesis (*23*) using the pMAL-ΔN102/ΔC24 vector (*14*) as a template. The following primers were used for PCR-based mutagenesis and DNA sequencing (mismatched nucleotides are shown in boldface and italic): F254A (forward), CTCTCGGGAT***GC***CTTGGGTGGCC; F254L (forward), TCGGGAT***C***TCTTGGGTGGCC; E286A (forward), ACCTGACATCTGCCATG***C***GCT; E286Q (forward), ACCTGACATCTGCCAT***C***AGCT; Y325F (forward), GAAAAGCTCGCCACAATTT***T***CT; B40(II) (inverse), CTGCCCATTCCTCATGTAGATTTCACTGTTAATGGAATCA; D (inverse), CTGCCCATTCCTCATGTAGA; A_{674} (forward), ATCCTGTGTACCGTGCAA; A_{641} (forward) (seq), CGGAACTGGATGCTGACCAC; $A3_{678}$ (forward) (seq), TGTGTACCGTGCAAGACG; $A2_{935}$ (forward) (seq), CTGGTTTCCGCCTCCGAC; $B2_{1172}$ (inverse) (seq), TATTCATCAGGTGCACCC; and B_{1564} (inverse) (seq), GGGCACTGCAAAGGATTCCA. Primer D is identical to the first 20 nucleotides of primer B40(II) which was taken from ref *14*. The truncated form of hPheOH (wild-type and mutants) proved to be less prone to aggregation and to be more stable than the corresponding full-length forms of the enzyme when expressed in *Escherichia coli.* Furthermore, the truncated wild-type form represents a fully activated state of the enzyme, and in contrast to the full-length enzyme, its activity is not regulated by either L-Phe or BH_4 (*14*). The target sequence for mutagenesis was the *Bam*HI−*Afl*II fragment of the hPheOH cDNA, and the authenticity of the mutagenesis was verified by DNA sequencing. DNA primers for PCR and DNA sequencing were synthesized on an Applied Biosystems (model 394) synthesizer. DyNAzyme II DNA polymerase used for PCR was from Finnzymes Oy. Samples for sequencing were prepared on a DNA Labstation 625 (Vistra systems) using the Labstation Thermo Sequenase labeled primer cycle sequencing kit with 7-deaza-dGTP (Amersham) and FITC-labeled primers. The DNA sequencing was carried out on an automatic DNA sequencer (A. L. F. DNA sequencer, Pharmacia Biotech), and the data were analyzed by means of the program ALFwin, version 1.00. The restriction endonucleases and the restriction protease factor Xa were from New England Biolabs.

Expression in E. coli and Purification of Recombinant hPheOH Forms. Wild-type and mutant forms of the doubly truncated dimeric form ΔN102/ΔC24-hPHeOH were ex-

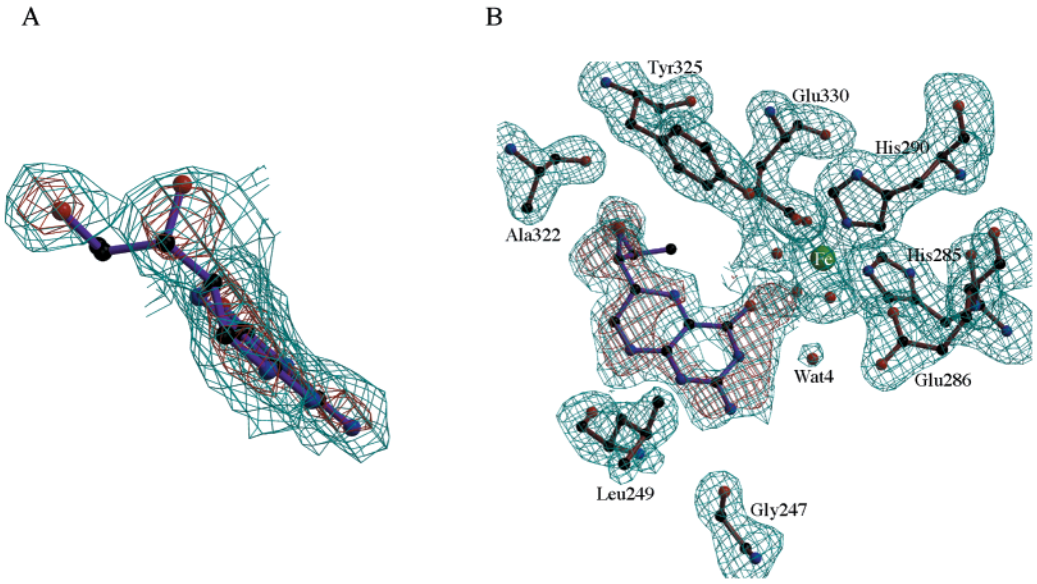

FIGURE 1: (A) Electron density for 7,8-BH_2 in the binary structure (side view). The map is an $F_{obs} - F_{calc}$ omit map contoured at 1.2σ (cyan) and 2.0σ (red). In this figure, BH_4 is modeled into the density to show the better fit at the C6 position of the pterin ring. (B) Electron density at the active site of the binary complex of doubly truncated hPheOH with 7,8-dihydro-L-biopterin (top view). The density around the pterin is an $F_{obs} - F_{calc}$ omit map (where the active site residues and the pterin have been omitted in the map calculation). Two contour levels are shown: 1.2σ (cyan) and 2.0σ (red). The figures were made using the program Bobscript (*52*).

pressed as fusion proteins in *E. coli* using the maltose-binding protein (MBP) as a fusion partner (*13*, *14*). After induction of hPheOH by 1 mM isopropyl thio-β-D-galactoside (IPTG), the cells were grown at 28 °C for 2, 8, and 24 h (however, no significant difference was observed in the kinetic properties of the enzymes obtained with different induction times). The fusion proteins were purified by affinity chromatography (amylose resin), followed by size-exclusion chromatography at 4 °C, using a HiLoad Superdex 200 HR column (1.6 cm $\times$ 60 cm), prepacked by Pharmacia (*13*). The dimeric fusion proteins were cleaved by the restriction protease factor Xa as described previously (*24*). The hPheOH activity was assayed as previously described (*24*). All the mutant forms revealed the formation of a normal catecholamine-to-iron charge-transfer complex characteristic of the wild-type form (*25*), as measured spectrophotometrically.

RESULTS AND DISCUSSION

Pterin Binding at the Active Site of hPheOH. Electron density difference maps (at 2σ) showed density that could be interpreted as the pterin ring, with continuous electron density toward the iron, and density for the dihydroxypropyl side chain of 7,8-dihydro-L-biopterin (BH_2) pointing toward Ala322. This allowed for the positioning of the pterin ring, as well as O4 and the dihydroxypropyl side chain. The final electron density for some interesting active site residues, including the pterin, is shown in Figure 1, as a CCP4 (*21*) difference ($F_{obs} - F_{calc}$) omit map contoured at 2.0σ (in red) and 1.2σ (in cyan).

The crystal structure of the binary complex can be superimposed on the crystal structure of the corresponding ligand-free native form (PDB file 1PAH) (*7*) with a root-mean-square (rms) displacement of 0.26 Å (C_α atoms of residues 118−424 used in the superimposition). If it is superimposed on the structure of the hPheOH−adrenaline inhibitor complex (PDB file 3PAH) (*25*), the rms displacement is similar (0.28 Å) to that with the native ligand-free form. Superimposition onto the corresponding region of rPheOH, which includes the regulatory domain (PDB file 2PHM) (*9*), can be done with a larger rms displacement (0.82 Å). All three rms displacement values are larger than the estimated coordinate error for the pterin-bound structure (0.23 Å) (Table 1). However, only the difference between rPheOH and the binary hPheOH·BH_2 complex is significant. This may be due to several factors. For example, it may reflect true differences between the nonactivated (rPheOH structure) and fully activated (hPheOH doubly truncated structure) forms of the enzyme, differences between the human and the rat enzyme, or even the different space groups in which the two structures crystallized (*9*, *15*).

The loop between residues 245 and 250 shows the largest displacements (the C_α atom of Gly247 moves ~1.3 Å toward the pterin ring), if compared to the native ligand-free structure (Figure 2). The loop between residues 245 and 250 moves in the direction of the iron and thus is able to form several hydrogen bonds (see Figure 3 and Tables 2 and 3) to the pterin ring. The pterin cofactor is thus in an ideal orientation for dioxygen to bind in a bridging position between the iron and the pterin. The Leu248 side chain changes its conformation as compared to the nonliganded structure, and now faces the active site. Leu255 also shifts its conformation to accommodate the dihydroxypropyl side chain of the pterin. Mutations in Gly247 (G247V), Leu249 (L249F/H), and Leu255 (L255V/S) have been reported in patients with phenylketonuria [PKU database located at http://www.mcgill.ca/pahdb (*24*, *26*)]. Considering the important hydrogen bonds between the cofactor and these active site residues (Figure 3 and Tables 2 and 3) as well as the movements Gly247 undergoes upon pterin binding, the dysfunction of the mutant enzyme forms can be easily understood. For example, expression analysis of G247V in COS cells has demonstrated that the mutant enzyme has no residual enzymatic activity (*27*).

The pterin ring forms aromatic π-stacking interactions with Phe254, as seen with the analogous residue Phe300 in the

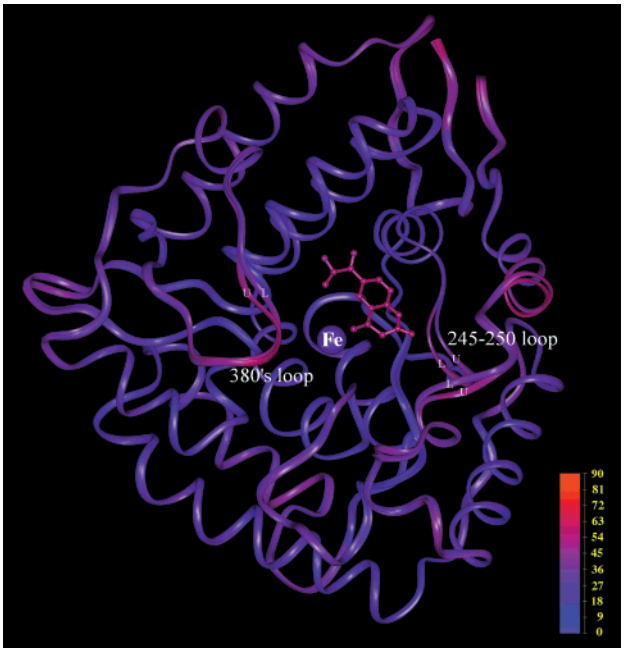

FIGURE 2: Superposition of the native doubly truncated form of hPheOH and the binary hPheOH·BH_2 complex. The *B*-factors of the individual C_α atoms of the main chain in the two structures are plotted as colored ribbons. The color scheme for the *B*-factors is shown to the bottom right. For clarity purposes, the loops exhibiting the largest differences between the liganded structure and the unliganded structure are marked with L and U, respectively.

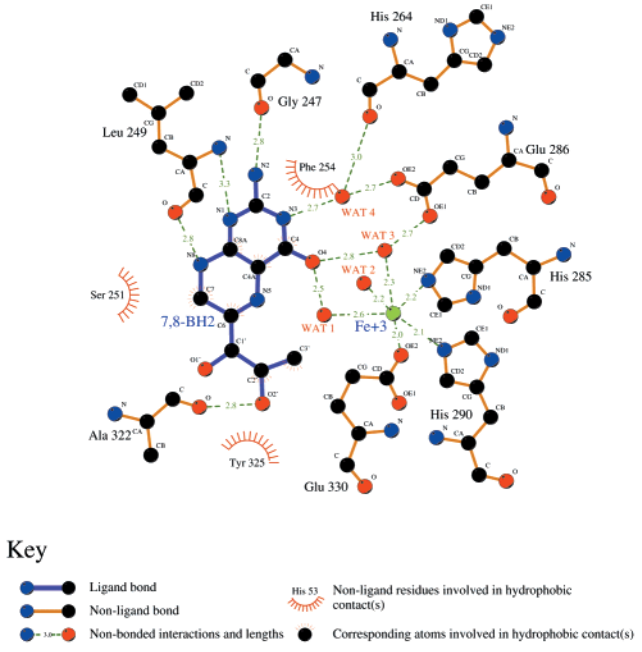

FIGURE 3: Specific interactions at the pterin and iron binding site of hPheOH. The figure was prepared with the program Ligplot (*53*). The pterin is shown in purple and the iron in green. Nitrogen atoms are colored blue; oxygen atoms and water molecules are red, and the carbon atoms are black.

pterin-bound form of rTyrOH (*11*). The average interatomic distance between the pterin and the benzene ring is 3.6 Å, and the pterin is about 10° offset from being parallel with the benzene ring of Phe254. No meta-hydroxylation is observed in the structure presented here, in contrast to the corresponding Phe300 residue in rTyrOH, consistent with

Table 2: Atomic Distances between the Active Site Iron, Its Ligated Water Molecules, and 7,8-Dihydro-L-biopterin

	distance (Å)		distance (Å)
Fe−O4	3.8	Fe−Wat1	2.6
Fe−C4a	6.1	Wat1−O4	2.5
Fe−N5	6.1	Wat3−O4	2.8
Fe−Wat3	2.3		

Table 3: Atomic Distances between Some Important Active Site Residues and 7,8-Dihydro-L-biopterin

	distance (Å)
N2−Gly247 (main chain C═O)	2.8
N1−Leu249 (main chain N)	3.3
N8−Wat5	3.2
N8−Leu249 (main chain C═O)	2.8
O10−Ala322 (main chain C═O)	2.8
N3−Wat4	2.7
Tyr325−Wat1	2.7
Glu286 Oϵ1−Wat3	2.7
Glu286 Oϵ2−Wat4	2.6

the previously determined hPheOH structures (*7*, *25*). Phe300 (in rTyrOH) has recently been reported to be mutated into an alanine (*28*), resulting in a 60% decrease in activity (using 6-methyltetrahydropterin as the cofactor). It was found that Phe300 contributes approximately 1 kcal/mol to the binding of tetrahydrobiopterin in rTyrOH, which is comparable to the interactions observed between aromatic amino acids and pyrimidines (*29*). In this study, when Phe254 was mutated into alanine in the doubly truncated form of hPheOH, the K'_m (BH_4) increased from 39 ± 6 to 72 ± 9 μM, whereas the V'_{max} was reduced to ~14% of the wild-type value (Table 4). Mutation to the hydrophobic leucine also resulted in a reduced affinity for BH_4, whereas the V'_{max} slightly increased.

A detailed picture of the interatomic distances and contacts that BH_2 makes with hPheOH is shown in Figure 3, and the distances are listed in Tables 2 and 3. The iron atom has an octahedral coordination geometry, with ligation by His285, His290, Glu330, and three water molecules, as in the nonliganded form (*7*). Two waters are located approximately equidistant between the iron and O4 of the pterin (Wat3 and Wat1), and the third is on the opposite side of the iron (Wat2), facing His290. Another water molecule is seen hydrogen bonded to N3 of the pterin ring at a distance of 2.7 Å (Wat4). This water molecule is further hydrogen bonded to Glu286, thus making important connections between this residue and the pterin. Glu286 has been identified as a critical residue for pterin function in full-length rPheOH (*30*), and when mutated in this doubly truncated form of hPheOH into an alanine, it shows a 50-fold increase in the K'_m for the natural pterin cofactor (Table 4). The V'_{max} is only 0.2% of the wild-type value (k'_{cat}/K'_m was 0.002 as compared to 69 for the wild-type form). The more conservative mutation E286Q revealed an only 1.4-fold increase in the K'_m value, but a V'_{max} of only ~2% of the wild-type value (k'_{cat}/K'_m was 1.3). Thus, Glu286 is important for the correct positioning of the pterin cofactor for catalysis. In the crystal structure presented here, Glu286 is located opposite Glu330 and 4.4 Å away from the iron, forming hydrogen bonds to one of the water molecules ligated to the iron, as well as a hydrogen bond to the water molecule (Wat4) that hydrogen bonds to N3 of the pterin ring. Both water molecules are seen in all of the previously

Table 4: Steady-State Kinetic Parameters of the Dimeric Catalytic Domain (Residues 103−424) of Human Phenylalanine Hydroxylase and Some of Its Active Site Mutations[a]

	BH_4		L-Phe		
enzyme form	K'_m (μM)	V'_{max} (nmol min^{-1} mg^{-1})	K'_m (μM)	V'_{max} (nmol min^{-1} mg^{-1})	substrate inhibition[c] (L-Phe)
wild-type	39 ± 6	6801 ± 365	91 ± 10	10343 ± 512	yes
F254A	72 ± 9	723 ± 19	595 ± 65[b]	1777 ± 60	no
F254L	163 ± 10	7225 ± 130	53 ± 15[b]	10714 ± 1121	yes (pronounced)
E286A	1936 ± 309	8.8 ± 0.6	35 ± 13[b]	6.6 ± 0.9	no
E286Q	53 ± 3	142 ± 3	488 ± 47[b]	126 ± 4	no
Y325F	38 ± 3	5010 ± 134	143 ± 13	3438 ± 103	yes

[a] The hPheOH activity was assayed, and the apparent kinetic constants were calculated by nonlinear regression analysis as described previously (*24*). The substrate concentrations were 1 mM L-Phe (BH_4 variable) and 75 μM BH_4 (L-Phe variable). [b] The final concentration of BH_4 was 750 μM (F254A and -L mutations) and 2 mM (E286A and -Q mutations). [c] Not considered in the determination of the kinetic constants.

determined crystal structures of the ligand-free form of hPheOH as well as in the catecholamine inhibitor complexes (*7*, *25*). The water molecule coordinated to both the iron and Glu286 (Wat3) shows the smallest *B*-factor (25.4 Å^2 as compared to 49.6 and 33.9 Å^2 for Wat1 and Wat2, respectively) of the three ligand water molecules in all hPheOH structures, and is thus likely to be the least mobile of the three. A water molecule that is ligated to the iron as well as to Glu332 is also observed in the same position in the ligand-free rTyrOH structure as well as its binary complex with BH_2 (*10*, *11*). Thus, this water molecule may be important for maintaining the active site geometry in the aromatic amino acid hydroxylases, and possibly, in cooperation with Glu286, in recognizing the pterin ring.

In all other pterin or pterin analogue binding enzymes that have been structurally characterized as binary complexes, the N3 atom interacts directly with the side chain carboxylate group of a charged amino acid (*31*, *32*). In nitric oxide synthase (NOS), N3 of the pterin cofactor interacts directly with the propionate group of heme A, regulating oxy-heme reactivity (*33*, *34*). Thus, no water molecule has previously been seen to interact with this part of the pterin ring in a protein crystal structure. The importance of water-mediated contacts in ligand binding specificity is well documented. In DNA-binding enzymes, like the tryptophan repressor (*35*, *36*) and the purine repressor PurR in complex with guanine and the *purF*-operator DNA (*37*), water-mediated hydrogen bonds to the ligand (DNA or guanine) are reported. In the PurR complex, this water-mediated ligand interaction is vital in discrimination between different corepressors. Other examples include the oligopeptide binding protein OppA (*38*, *39*) and L-arabinose binding protein (*40*).

In addition to the previously mentioned water molecules and Glu286, there are several interactions between the pterin and the protein on the other side of the pterin molecule, pointing away from the iron. As mentioned above, this is the region of the protein that undergoes the largest movements upon pterin binding, and is thus involved in recognizing the pterin as a cofactor. The N1 and N8 pterin atoms form hydrogen bonds to the amide backbone of Leu249 at distances of 3.3 and 2.8 Å, respectively. N2 also makes a strong hydrogen bond to the main chain carbonyl oxygen of Gly247 at a distance of 2.8 Å. The dihydroxypropyl side chain interacts with the main chain carbonyl oxygen of Ala322 through a strong hydrogen bond with O10 (2.8 Å). The dihydroxypropyl side chain has previously been observed to have an almost cis conformation of the two hydroxyl groups at C1′ and C2′ in the binary complex of rat TyrOH (*41*). This is also seen in the binary complex of hPheOH, with a torsional angle between the hydroxyl groups of ∼53°. Mutations of Ala322 (A322T and A322G), associated with mild forms of hyperphenylalaninemia, have been reported to result in kinetic variant forms of the enzyme based on expression in a eukaryotic cell system (*42*).

The side chain of Tyr325, which is in proximity to the iron (O−Fe, 4.5 Å) in the ligand-free structure and highly conserved in the aromatic amino acid hydroxylases, is hydrogen bonded (2.7 Å) to Wat1. In the binary complex, the phenyl ring of Tyr325 establishes hydrophobic contacts with the C3′ methyl group of the dihydroxypropyl side chain of the pterin, and thus contributes to the correct positioning of the pterin cofactor for catalysis. When Tyr325 was mutated to phenylalanine, no significant change was observed for the K'_m value (BH_4) whereas the V'_{max} value slightly decreased with both BH_4 and L-Phe as the variable substrate (Table 4). This finding supports the stabilizing hydrophobic contacts of an aromatic amino acid at this position with the pterin but excludes the suggested possibility (*7*) of a direct functional role of Tyr325 in catalysis, in agreement with the results obtained with rTyrOH (*43*). The significance of a stabilizing aromatic residue (Tyr or Phe) in position 325 is further supported by the finding that the mutation Y325C (genotype Y325C/L348V) is associated with classical phenylketonuria [PKU database at http://www.mcgill.ca/pahdb (*26*)].

After refinement, the electron density shows the pterin ring to be surprisingly nonplanar (Figure 1). First, C6 can be modeled into the maps with a chair conformation (Figure 1A), similar to the X-ray structures of tetrahydrobiopterin (*44*) and 5,6,7-trimethyl-5,6,7,8-tetrahydrobiopterin dihydrochloride monohydrate (*45*), without any change in the *R*-factors of the model, but providing a better fit to the observed density. Second, the density also suggests that C2 of the theoretically aromatic (thus planar) pyrimidine ring is slightly out of the plane (about 0.8 Å) of the pterin. In the crystal structures of 6-methyl-7,8-dihydropterin monohydrochloride monohydrate (*46*) and xanthopterin hydrochloride (*47*), the pyrimidine ring is strictly planar. A possible explanation for the observed nonplanarity of the pterin ring could be that, to form the optimal angle for hydrogen bonding to the main chain carbonyl oxygen of Gly247, C2 has to be slightly bent out of the plane of the pterin ring (induced fit). This may represent an optimal positioning of the pterin ring for catalysis. The current model has been refined as planar in this position (with an angle between the plane of the pterin and the carbonyl oxygen of ∼110°). To definitively determine the question of planarity at this position in the pterin

ring, diffraction data to a resolution higher than 2.0 Å are required.

Structural Insight into the Effects of Pterin Substitutions on the Catalytic Activity and Regulatory Properties of PheOH. A number of different pterins can be used by PheOH as the cofactor in the hydroxylation reaction (*1*, *2*). In general, the pyrimidine portion of the pterin ring seems most essential for cofactor activity (*1*, *2*). This can be explained by the strong hydrogen bonds between N2 and N1 and active site amino acid residues (Gly247 and Leu249). A strong hydrogen bond is also seen between N3 and Wat4 (Figure 3). On the other hand, the pyrazine ring is not strictly important for cofactor activity, as found in a study with effective (albeit with a lower rate than BH_4) pteridines such as 2,5,6-triamino-4-pyrimidinone and 5-benzyl-2,6-diamino-4-pyrimidone (*48*). This can be interpreted with the crystal structure presented here by observing that there are few interactions between this portion of the pterin ring and the protein [only N8 makes a strong hydrogen bond to the protein (Leu249) and a water molecule]. The stereochemistry of the dihydroxypropyl side chain in the C6 position has been determined to be 6*R* (*44*). However, the 6*S* configuration and a range of 6-substituted tetrahydrobiopterins can also function as the cofactor (*1*). Relatively large differences in catalytic activity and coupling efficiency have been reported between the aromatic amino acid hydroxylases when various 6-substituted pterins are used as the electron donor (*2*). This could explain the differences found both in the binding of pterin analogues (*11*) and in their regulatory properties in the hydroxylases (*4*).

Although several cofactor analogues support the hydroxylation reaction catalyzed by full-length PheOH, only the natural cofactor (BH_4) functions as an efficient inhibitor of the L-Phe-induced activation of the enzyme (*2*). The molecular mechanism of this inhibition is not yet understood (*2*, *4*, *9*). BH_2 inhibits the activation by L-Phe less efficiently than BH_4 (*49*). The strong hydrogen bond seen between the dihydroxypropyl side chain of BH_2 (O2′ atom) and the protein (carbonyl oxygen of Ala322), in combination with the conformational changes of the polypeptide chain (loop between residues 245 and 250) observed upon BH_2 binding, could provide an explanation as to why the dihydroxypropyl side chain is required for inhibition. These results are also compatible with a specific regulatory function of the natural cofactor by its binding at the active site. Interestingly, when the structure of the binary complex hPheOH·BH_2 presented here is superimposed onto the crystal structure of the ligand-free rPheOH (containing the regulatory domain) (*9*), BH_2 is seen to interact with the N-terminal autoregulatory sequence. This autoregulatory sequence does not contain the phosphorylation site Ser16 in the crystal structure itself, but one may speculate that Ser16 is extending over the active site pocket. The catalytic domains of the two structures overlap with a rms deviation of 0.82 Å, and the dihydroxypropyl side chain (C2′-hydroxyl group) is sufficiently close in the superposition (2.7 Å at the shortest) to form hydrogen bonds to Ser23 (through either the side chain or the carbonyl oxygen of the main chain) (Figure 4). Thus, upon BH_4/BH_2 binding in the full-length PheOH, a conformational change of the protein, including a movement of the mobile N-terminal autoregulatory sequence (*9*), is likely to occur, forming the proper length hydrogen bonds to the pterin. This model gives a plausible structural explanation for the inhibitory effect of BH_4 binding on the rate of phosphorylation of Ser16 in rPheOH by cAMP-dependent protein kinase, which is relatively specific for the *R*-isomer of the natural cofactor (BH_4) with its dihydroxypropyl side chain (*50*). Furthermore, on phosphorylation of Ser16, the mobile autoregulatory sequence may undergo further movement, which facilitates the access of L-Phe to the active site. This conclusion is consistent with the experimental finding that the phosphorylated form of rPheOH requires less L-Phe to be activated ($S_{0.5} = 29\ \mu M$) than the nonphosphorylated form ($S_{0.5} = 51\ \mu M$) (*50*). Thus, to explain the regulatory properties of BH_4 in the full-length form of PheOH, it is not necessary to have an additional binding site of the cofactor in the regulatory domain as recently postulated (*9*).

A similar location of BH_2 in hPheOH has been proposed on the basis of ^1H NMR spectroscopy and molecular docking (*51*) and observed in rTyrOH on the basis of the 2.3 Å resolution crystal structure (*11*). In both structures, the pterin molecule is surrounded predominantly by backbone protein atoms located in the loop region of residues 245−250 in hPheOH and 291−296 in rTyrOH. In the hPheOH·BH_2 crystal structure, the pterin molecule is held in place by seven hydrogen bonds and three side chain hydrophobic interactions (Figure 3). In comparison to the rTyrOH·BH_2 structure (*11*), the pterin C4a atom, which becomes hydroxylated during the enzymatic reaction, is in a very similar location with a C4a−Fe distance of 6.1 Å (5.6 Å in rTyrOH). However, the pterin molecule in the rTyrOH·BH_2 structure (*11*) has an orientation rotated 180° around the central C4a−C8a bond relative to that in the hPheOH·BH_2 crystal structure. This difference in orientation may partly be explained by two different conformational binding sites in the two enzymes, an effect of different crystallization conditions, or incorrect positioning of the pterin molecule in the TyrOH·BH_2 structure (*11*). The resolution of the PheOH·BH_2 structure is 2.0 Å which is higher than that of the TyrOH·BH_2 structure (2.3 Å), and the electron density is more well defined in the PheOH·BH_2 structure. Recent enzyme kinetic and molecular docking studies on TyrOH with 20 synthetic analogues of BH_4 (substituents at the C2, N3, C4, N5, C6, and C7 positions) all support the orientation of the pterin in the hPheOH structure (B. Almås, K. Toska, K. Teigen, V. Groehn, W. Pfleiderer, A. Martinez, T. Flatmark, and J. Haavik, personal communication). In the "NMR structure" of the hPheOH·BH_2 binary complex, the pterin molecule is observed to be closer to the iron atom than in the crystal structure (Table 2), with the C4a at a distance of ∼4.3 Å (*51*). The proposed direct binding of the pterin to the iron atom in the NMR structure (*51*) could be due to the inability of ^1H NMR to identify active site residues or account for the observed movement of the loop between residues 245 and 250, and the inherent limitations of the molecular docking procedure. All other biochemical studies with pterin analogues are consistent with the orientation of BH_2 observed in the hPheOH·BH_2 crystal structure presented here (*2*).

Comparison of Binding Sites of L*-Phenylalanine, Catecholamine Inhibitors, and Pterins in hPheOH.* The doubly truncated form of hPheOH used in this study for crystallization and mutagenesis represents a fully activated form of the enzyme. In contrast to that of the full-length form of hPheOH, its catalytic activity is not regulated either by L-Phe or by BH_4. Thus, substrates have free access to the active

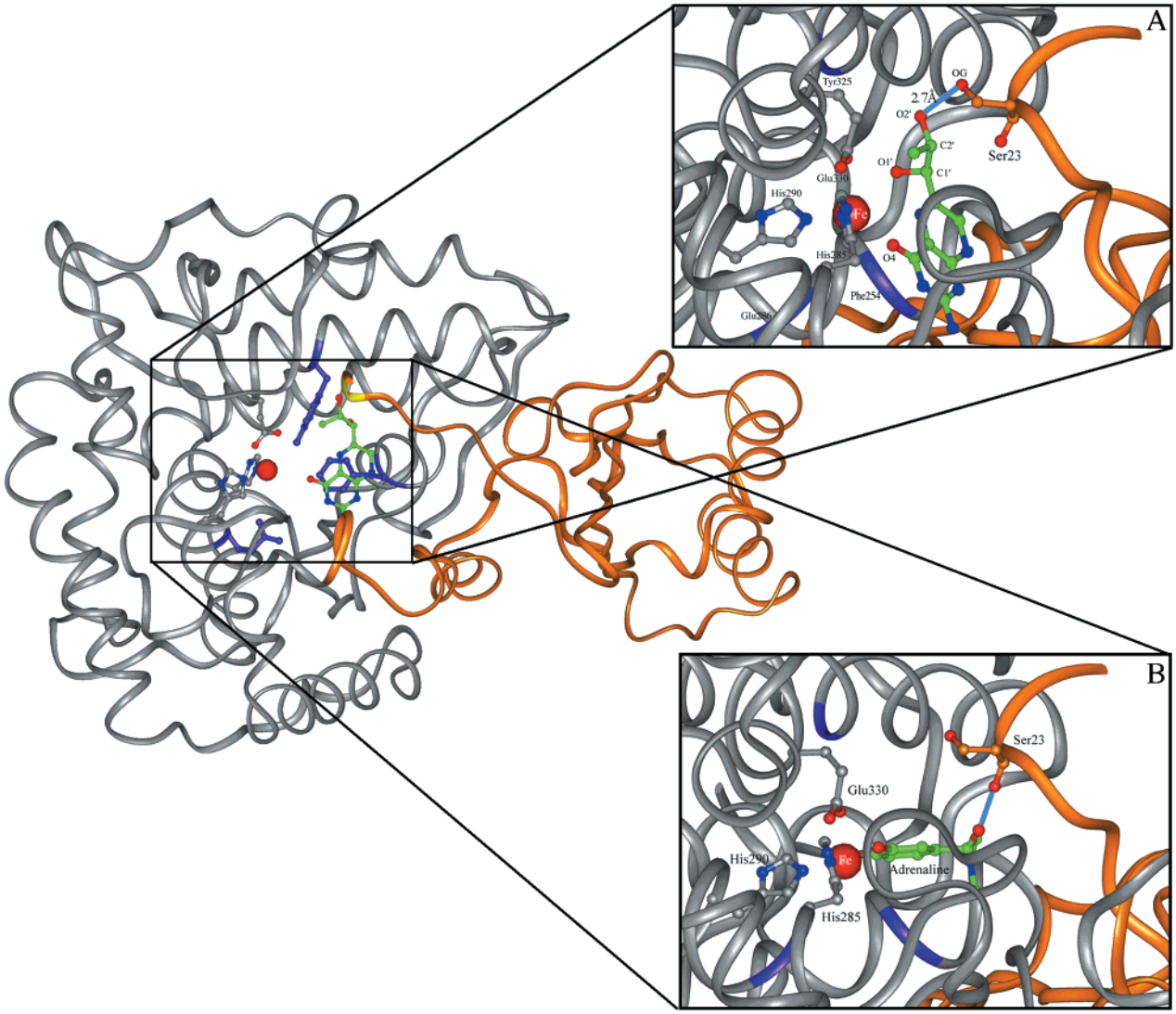

FIGURE 4: Putative interactions of the N-terminal autoregulatory sequence of rPheOH with the pterin. The hPheOH·BH_2 structure was superimposed onto the corresponding region (residues 118−424) of the ligand-free rPheOH structure (PDB file 2PHM) containing the regulatory and catalytic domains. The residues mutated in the study presented here are shown in purple. Displayed in this figure is the C_α ribbon of the protein backbone from the rat PheOH structure, together with the pterin and the iron from the hPheOH·BH_2 structure. (A) An enlargement of the active site is also shown. Residues that have been mutated in the work presented here are colored purple. The side chains are not shown for clarity. (B) Corresponding active site enlargement (as in panel A) of the putative interactions of the adrenaline molecule (PDB file 3PAH) with the N-terminal regulatory domain.

site, and the apparent affinity for L-Phe is increased (ref *14* and Table 4). However, the substrate inhibition (L-Phe) of the doubly truncated form is more pronounced than that observed for the full-length enzyme (*14*). A strong substrate inhibition (comparable to that of the wild-type doubly truncated form) was found for two mutant forms (F254L and Y325F) which have preserved a relatively high affinity for L-Phe (Table 4). On the other hand, in Table 4 it is seen that mutations in Phe254 (F254A) and Glu286 (E286A and E286Q) change not only the binding affinity of BH_4 but also that of L-Phe. The largest effects were observed for the F254A and E286Q mutations, in which the K'_m values (L-Phe) increased 7- and 5-fold, respectively, with only a slight decrease in the affinity for the cofactor. In contrast, a reduced K'_m (L-Phe) was observed for the F254L mutant. Thus, mutations in residues that in the crystal structure strongly interact with the pterin cofactor will also affect the binding of the L-Phe in different ways. How these mutations affect the binding of L-Phe will only be known when the exact binding site for L-Phe in hPheOH is determined by a crystal structure of the binary or ternary complex with L-Phe.

Interestingly, an overlay of the hPheOH·adrenaline structure (*25*) and the hPheOH·BH_2 structure presented here (Figure 5) revealed that several atoms are within van der Waals distances (C6, C7, and C9 of adrenaline are approximately 1 Å from N5, N1, and N1, respectively). When the hPheOH·adrenaline structure is superimposed onto the crystal structure of the ligand-free rPheOH (containing the regulatory domain) (*9*), adrenaline is seen to interact with the N-terminal autoregulatory sequence (Figure 4B). Steric interactions between the Cβ atom of the adrenaline molecule and the carbonyl oxygen of Ser23 and the Leu25 side chain are observed irrespective of the orientation in which the catecholamine molecule is bound to the ferric iron. These interactions with the N-terminal autoregulatory sequence are similar to those made with the pterin cofactor as mentioned

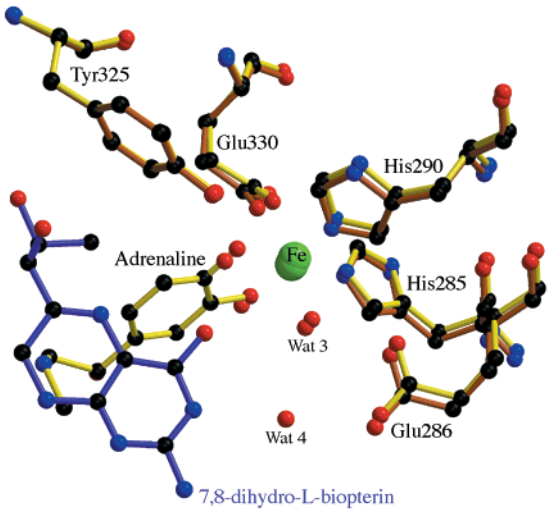

FIGURE 5: Superposition of the two structures of hPheOH with bound adrenaline and bound 7,8-BH_2, respectively. The adrenaline structure has been colored yellow, and the protein side chains of the pterin structure are brown. The pterin is shown in purple and the iron in green. Nitrogen atoms are colored blue; oxygen atoms and water molecules are red, and the carbon atoms are black. The figure was prepared using the programs Molscript (*54*) and Raster3D (*55*).

in the previous section. Correspondingly, this gives a plausible structural explanation for the observed inhibitory effect of catecholamine binding on the rate of phosphorylation of Ser16 in full-length hPheOH by cAMP-dependent protein kinase, which is quantitatively similar to the inhibition observed with BH_4 as the negative effector (T. Solstad and T. Flatmark, unpublished data).

ACKNOWLEDGMENT

The mass spectroscopy facility and Drs. Laura B. Pasternack and Dee-Hua Huang at the NMR facility of The Scripps Research Institute are greatly acknowledged for performing the studies of 7,8-BH_2 in solution. Ali S. Munoz and Randi M. Svebak are acknowledged for their expert technical assistance in preparing large amounts of pure protein for crystallization, and Dr. Anne-Brit Kolstø is acknowledged for support in the site-directed mutagenesis. Albert E. Beuscher, Dr. Marianne G. Patch, and Dr. Enrique Abola are thanked for their help and discussions in preparation of the manuscript.

REFERENCES

1. Kaufman, S. (1993) *Adv. Enzymol. 70*, 77−264.
2. Kappock, T. J., and Caradonna, J. P. (1996) *Chem. Rev. 96*, 2659−2756.
3. Hufton, S. E., Jennings, I. G., and Cotton, R. G. H. (1995) *Biochem. J. 311*, 353−366.
4. Flatmark, T., and Stevens, R. C. (1999) *Chem. Rev. 99*, 2137−2160.
5. Hegg, E. L., and Que, L. (1997) *Eur. J. Biochem. 250*, 625−629.
6. Lange, S. J., and Que, L. J. (1998) *Curr. Opin. Chem. Biol. 2*, 159−172.
7. Erlandsen, H., Fusetti, F., Martinez, A., Hough, E., Flatmark, T., and Stevens, R. C. (1997) *Nat. Struct. Biol. 4*, 995−1000.
8. Fusetti, F., Erlandsen, H., Flatmark, T., and Stevens, R. C. (1998) *J. Biol. Chem. 273*, 16962−16967.
9. Kobe, B., Jennings, I. G., House, C. M., Michell, B. J., Goodwill, K. E., Santarsiero, B. D., Stevens, R. C., Cotton, R. G. H., and Kemp, B. E. (1999) *Nat. Struct. Biol. 6*, 442−448.
10. Goodwill, K. E., Sabatier, C., Marks, C., Raag, R., Fitzpatrick, P. F., and Stevens, R. C. (1997) *Nat. Struct. Biol. 4*, 578−585.
11. Goodwill, K. E., Sabatier, C., and Stevens, R. C. (1998) *Biochemistry 37*, 13437−13445.
12. Jennings, I. G., Kemp, B. E., and Cotton, R. G. H. (1991) *Proc. Natl. Acad. Sci. U.S.A. 88*, 5734−5738.
13. Martinez, A., Knappskog, P. M., Olafdottir, S., Døskeland, A. P., Eiken, H. G., Svebak, R. M., Bozzini, M., Apold, J., and Flatmark, T. (1995) *Biochem. J. 306*, 589−597.
14. Knappskog, P. M., Flatmark, T., Aarden, J. M., Haavik, J., and Martinez, A. (1996) *Eur. J. Biochem. 242*, 813−821.
15. Erlandsen, H., Martinez, A., Knappskog, P. M., Haavik, J., Hough, E., and Flatmark, T. (1997) *FEBS Lett. 406*, 171−174.
16. Fukushima, T., and Akino, M. (1968) *Arch. Biochem. Biophys. 28*, 1−5.
17. Otwinowski, Z., and Minor, W. (1996) *Methods Enzymol. 276*, 307−326.
18. Brunger, A. T., Adams, P. D., Clore, G. M., DeLano, W. L., Gross, P., Grosse-Kunstleve, R. W., Jiang, J.-S., Kuszewski, J., Nilges, M., Pannu, N. S., Read, R. J., Rice, L. M., Simonson, T., and Warren, G. L. (1998) *Acta Crystallogr. D54*, 905−921.
19. Brunger, A. T. (1992) *Nature 355*, 472−475.
20. Jones, T. A., Zou, J.-Y., Cowan, S. W., and Kjeldgaard, M. (1991) *Acta Crystallogr. A47*, 110−119.
21. CCP4 (1979) *A suite of programs for Protein Crystallography*, SERC Daresbury Laboratory, Warrington, U.K.
22. Hodel, A., Kim, S.-H., and Brunger, A. T. (1992) *Acta Crystallogr. A48*, 851−858.
23. Nelson, R. M., and Long, G. L. (1989) *Anal. Biochem. 180*, 147−151.
24. Bjørgo, E., Knappskog, P. M., Martinez, A., Stevens, R. C., and Flatmark, T. (1998) *Eur. J. Biochem. 257*, 1−10.
25. Erlandsen, H., Flatmark, T., Stevens, R. C., and Hough, E. (1998) *Biochemistry 37*, 15638−15646.
26. Nowacki, P., Byck, S., Prevost, L., and Scriver, C. R. (1998) *Nucleic Acids Res. 26*, 220−225.
27. Li, J., Eisensmith, R. C., Wang, T., Lo, W. H., Huan, G. S. Z., Zeng, Y. T., Yuan, L. F., Liu, S. R., and Woo, S. L. (1992) *Genomics 13*, 894−895.
28. Ellis, H. R., Daubner, S. C., McCulloch, R. I., and Fitzpatrick, P. F. (1999) *Biochemistry 38*, 10909−10914.
29. Shamoo, Y., Ghosaini, L. R., Keating, K. M., Williams, K. R., Sturtevant, J. M., and Konigsberg, W. H. (1989) *Biochemistry 28*, 7409−7417.
30. Dickson, P. W., Jennings, I. G., and Cotton, R. G. (1994) *J. Biol. Chem. 269*, 20369−20375.
31. Auerbach, G., Herrmann, A., Gutlich, M., Fischer, M., Jacob, U., Bacher, A., and Huber, R. (1997) *EMBO J. 16*, 7219−7230.
32. Hampele, I. C., D'Arcy, A., Dale, G. E., Kostrewa, D., Nielsen, J., Oefner, C., Page, M. G. P., Sconfeld, H.-J., Stuber, D., and Then, R. L. (1997) *J. Mol. Biol. 268*, 21−30.
33. Crane, B. R., Arvai, A. S., Ghosh, D. K., Wu, C., Getzoff, E. D., Stuehr, D. J., and Tainer, J. A. (1998) *Science 279*, 2121−2126.
34. Raman, C. S., Li, H., Martasek, P., Kral, V., Masters, B. S. S., and Poulos, T. L. (1998) *Cell 95*, 939−950.
35. Otwinowski, Z., Schevitz, R. W., Zhang, R.-G., Lawson, C. L., Joachimiak, A., Marmorstein, R. Q., Luisi, B. F., and Sigler, P. B. (1988) *Nature 335*, 321−329.
36. Joachimiak, A., Haran, T. E., and Sigler, P. B. (1994) *EMBO J. 13*, 367−372.
37. Schumacher, M. A., Glasfeld, A., Zalkin, H., and Brennan, R. G. (1997) *J. Biol. Chem. 272*, 22648−22653.
38. Tame, J. R. H., Sleigh, S. H., Wilkinson, A. J., and Ladbury, J. E. (1996) *Nat. Struct. Biol. 3*, 998−1001.

39. Sleigh, A. H., Tame, J. R. H., Dodson, E. J., and Wilkinson, A. J. (1997) *Biochemistry 36*, 9747−9758.
40. Quiocho, F. A., Wilson, K. A., and Vyas, N. K. (1989) *Nature 340*, 404−407.
41. Martinez, A., Vageli, O., Pfleiderer, W., and Flatmark, T. (1998) *Pteridines 9*, 44−52.
42. Svensson, E., Eisensmith, R. C., Dworniczak, B., von Dobeln, U., Hagenfeldt, L., Horst, J., and Woo, S. L. (1992) *Hum. Mutat. 1*, 129−137.
43. Daubner, S. C., and Fitzpatrick, P. F. (1998) *Biochemistry 37*, 16440−16444.
44. Matsuura, S., Sugimoto, T., Murata, S., Sugawara, Y., and Iwasaki, H. (1985) *J. Biochem. 98*, 1341−1348.
45. Bieri, J. H., and Viscontini, M. (1977) *Helv. Chim. Acta 60*, 1926−1931.
46. Bieri, J. H. (1977) *Helv. Chim. Acta 60*, 2303−2308.
47. Bieri, J. H., Hummel, W.-P., and Viscontini, M. (1976) *Helv. Chim. Acta 59*, 2374−2382.
48. Bailey, S. W., and Ayling, J. E. (1978) *Biochem. Biophys. Res. Commun. 85*, 1614−1621.
49. Døskeland, A. P., Haavik, J., Flatmark, T., and Døskeland, S. O. (1987) *Biochem. J. 242*, 867−874.
50. Døskeland, A. P., Døskeland, S. O., Øgreid, D., and Flatmark, T. (1984) *J. Biol. Chem. 259*, 11242−11248.
51. Teigen, K., Frøystein, N. Å., and Martinez, A. (1999) *J. Mol. Biol. 293*, 807−823.
52. Esnouf, R. M. (1997) *J. Mol. Graphics 15*, 132−134.
53. Wallace, A. C., Laskowski, R. A., and Thornton, J. M. (1995) *Protein Eng. 8*, 127−134.
54. Kraulis, P. J. (1991) *J. Appl. Crystallogr. 24*, 946−950.
55. Merritt, E. A., and Bacon, D. J. (1997) *Methods Enzymol. 277*, 505−524.

BI992531+